

Geostatistical space-time mapping of house prices using Bayesian maximum entropy

Darren K. Hayunga & Alexander Kolovos

To cite this article: Darren K. Hayunga & Alexander Kolovos (2016) Geostatistical space-time mapping of house prices using Bayesian maximum entropy, International Journal of Geographical Information Science, 30:12, 2339-2354, DOI: [10.1080/13658816.2016.1165820](https://doi.org/10.1080/13658816.2016.1165820)

To link to this article: <https://doi.org/10.1080/13658816.2016.1165820>



View supplementary material [↗](#)



Published online: 07 Apr 2016.



Submit your article to this journal [↗](#)



Article views: 651



View related articles [↗](#)



View Crossmark data [↗](#)



Citing articles: 3 View citing articles [↗](#)



Geostatistical space–time mapping of house prices using Bayesian maximum entropy

Darren K. Hayunga^a and Alexander Kolovos^b

^aDepartment of Insurance, Legal Studies, and Real Estate, University of Georgia, Athens, GA, USA;

^bSpaceTimeWorks, San Diego, CA, USA

ABSTRACT

Mapping spatial processes at a small scale is a challenge when observed data are not abundant. The article examines the residential housing market in Fort Worth, Texas, and builds price indices at the inter- and intra-neighborhood levels. To accomplish our objectives, we initially model price variability in the joint space–time continuum. We then use geostatistics to predict and map monthly housing prices across the area of interest over a period of 4 years. For this analysis, we introduce the Bayesian maximum entropy (BME) method into real estate research. We use BME because it rigorously integrates uncertain or secondary soft data, which are needed to build the price indices. The soft data in our analysis are property tax values, which are plentiful, publicly available, and highly correlated with transaction prices. The results demonstrate how the use of the soft data provides the ability to map house prices within a small areal unit such as a subdivision or neighborhood.

ARTICLE HISTORY

Received 14 November 2015

Accepted 10 March 2016

KEYWORDS


Spatiotemporal;
geostatistics; kriging;
Bayesian maximum entropy;
real estate

1. Introduction

Geographical immobility is one of the characteristics, that distinguishes housing from most other goods and services in the economy. The fact that a house has a unique signature encourages study of the impact spatial processes have on residential markets and specifically the effect on house values. This article examines the evolution of house prices over space and time at the inter- and intra-neighborhood levels. Our methods build more granular price indices than those currently available that focus at metropolitan levels.

In addition to measuring the overall price movements, another application of spatiotemporal price indices at small areal units is to investigate the level of variability within areas that exhibit similar socioeconomic characteristics. Goodman (1977) defines neighborhoods as small urban areas with a common set of socioeconomic effects. It is thus common for subdivision or neighborhood inhabitants to have similar incomes and education levels. Homes in these locations also experience similar separation distances from amenities like employment and shopping and disamenities such as traffic or noise

CONTACT Alexander Kolovos  alexander.kolovos@spacetimeworks.com

 Supplemental data for this article can be accessed [here](#).

© 2016 Informa UK Limited, trading as Taylor & Francis Group

pollution. But, it is an empirical question as to how much the neighborhood composition will affect prices in contrast to specific home attributes, as well as the level of price variability across neighborhoods.

To build a small-scale price index requires sampling and price predictions at unobserved locations and mapping the evolution of values over both space and time. The objectives of our analysis thus motivate the use of geostatistical approaches. There are a few papers that use the geostatistics methods of kriging and cokriging to model housing prices.¹ These include Dubin (1998), Chica-Olmo (2007), Páez *et al.* (2008), and Yoo and Kyriakidis (2009). Recently, Kuntz and Helbich (2014) compares univariate and multivariate kriging variants in real estate price mapping.

In this study, we employ Bayesian maximum entropy (BME) because it offers improvements over other methods.² The main advantage is that BME can properly incorporate uncertain data structures such as interval observations and probabilistic distributions. We find it a necessary condition to include soft data at the neighborhood level where the number of actual transactions is limited over a relevant time period. Since transactions are few, we augment with property tax data, which are ubiquitous, publicly available, and highly correlated with market prices, but are measured with uncertainty. Although kriging variants such as cokriging (e.g., Christakos 1992, Goovaerts 1997) can include secondary attribute observations for geostatistical prediction, classical geostatistical methodologies are unable to precisely or efficiently account for data uncertainty (Goovaerts 1997, Savelyeva *et al.* 2010). Our work illustrates the first application of BME in real estate research.³

Another contribution of our work is expressing price variability as a phenomenon in the joint space–time continuum. Much of the housing literature employs spatial econometrics only, usually hedonic models with spatial weight matrices to control for autocorrelation and heteroscedasticity. LeSage and Pace (2009) provides a comprehensive text on models and advances in this literature. Nappi-Choulet and Maury (2011) is the first housing paper to control for temporal autocorrelation and heteroscedasticity along with spatial autocorrelation and heteroscedasticity using hedonic modeling. Consistent with the literature using hedonic models, the focus is on controlling or removing the spatial and temporal processes from the models. Our analysis instead specifically uses these information sets to build the price index.

In addition to space being the primary focus, time in real estate applications has been hereto examined as a separate dimension outside the composite spatiotemporal domain (e.g., Banerjee *et al.* 2004, Montero and Larraz 2011). Gelfand *et al.* (2004) is one of the first housing papers to consider the temporal element, albeit within a time series context rather than as an integral vector in the evolution of housing prices in space–time. Transaction prices evolve in the space–time continuum, hence it is important to account correctly for the particular characteristics of spatiotemporal geometry to provide a more complete description of the attribute. Otherwise, by arbitrarily considering space and time to be unrelated to each other, the analyst ignores the potential physical-based correlation that can exist due to evolution in the joint space–time continuum (Christakos *et al.* 2000). To properly model time along with the spatial component in residential real estate, we process the spatial and temporal vectors jointly to establish the price index correlation in space–time by means of spatiotemporal covariances. To the best of our knowledge, it is the first time in real estate research that the pricing correlation is established by means of a spatiotemporal distance vector.

We investigate two housing cases using BME in this study.⁴ Case A focuses on a homogeneous subset of sales transactions. Market participants (i.e., appraisers, owners, and investors) determine value based on similar comparable properties, therefore Case A examines a practical refinement of the observed data. Case B applies our approach to build a small-scale price index for an area similar in size to a neighborhood. For completeness, a third Case C uses the entire sample of transactions. This is a base case that we present separately as Supporting Information.

The logical framework of this article continues as follows. In [Section 2](#), we briefly describe the BME framework. In [Section 3](#), we explain the experimental design, which details the data and the housing test cases. [Section 4](#) provides the empirical results and [Section 5](#) concludes.

2. The BME space–time mapping framework

We begin with a general stochastic representation of the evolution of housing prices in space S and time T . As first shown by Christakos (1991), we consider transaction prices in a spatiotemporal random field (S-TRF) denoted as $X(\mathbf{p})$, $\mathbf{p} = (\mathbf{s}, t)$, where $\mathbf{s} = (s_1, s_2)$ is the spatial location vector with coordinates s_1 and s_2 , and t is the time variable. Price variability manifests as all possible realizations of $X(\mathbf{p})$ values across space–time points \mathbf{p} . The S-TRF assigns to each of these realizations a probability that depends on \mathbf{p} , and is fully defined when the distribution of the transaction price random variable $x(\mathbf{p})$ is known at all locations \mathbf{p} in the spatiotemporal continuum $\mathcal{E} = S \times T$. In the S-TRF context, inter-point distances in \mathcal{E} are defined on the basis of a joint space–time metric $d\mathbf{p}$. For a spatial distance $|d\mathbf{s}|$ and a time interval dt , the segment length $|d\mathbf{p}|$ between two spatiotemporal locations \mathbf{p}_1 and $\mathbf{p}_2 = \mathbf{p}_1 + d\mathbf{p}$ on the Euclidian plane is $|d\mathbf{p}| = \sqrt{d\mathbf{s}^2 + (vdt)^2}$, where v is a spatiotemporal metric coefficient (Christakos *et al.* 2000).

BME integrates multi-sourced information in three consecutive stages known as the prior, specificatory and posterior. In the prior stage, the analyst considers all relevant available general knowledge bases (G-KB), which include theoretical and empirical expressions of the $X(\mathbf{p})$ characteristics. An example of G-KB is a surface trend, denoted by the S-TRF expectation $m_x(\mathbf{p}) = \overline{X(\mathbf{p})}$, which represents systematic spatiotemporal patterns at a level larger than the study scale. Another example of G-KB is expressing spatiotemporal variability between space–time points \mathbf{p} and \mathbf{p}' by means of the covariance $c_x(\mathbf{p}, \mathbf{p}') = \overline{[X(\mathbf{p}) - m_x(\mathbf{p})][X(\mathbf{p}') - m_x(\mathbf{p}')]}$. The surface trend and covariance function express the first- and second-order statistical moments of an S-TRF. The BME framework foundation accounts for higher order moments, multipoint statistics, and additional relevant G-KB types such as physical laws and empirical models. For this study, the available G-KB consists of transaction prices trend and covariance information.

On the basis of the G-KB, the BME prior stage results in a map of probability density functions (PDFs) that quantify the distributions f_G of the prior probabilities. By designating an individual S-TRF realization as χ , the prior PDF is defined by

$$f_G(\chi, \mathbf{p})d\chi = \text{Prob}[\chi \leq X(\mathbf{p}) \leq \chi + d\chi]. \quad (1)$$

A concise description of the prior stage is given by the first fundamental BME equation

$$\int d\chi (\mathbf{g} - \bar{\mathbf{g}}) e^{\boldsymbol{\mu}^T \mathbf{g}} = 0, \quad (2)$$

where \mathbf{g} is a vector of N_c g_α -functions, $\alpha = 1, 2, \dots, N_c$, that represents the G-KB, and $\boldsymbol{\mu}$ is a vector of μ_α -coefficients that depends on the space-time coordinates and associates with \mathbf{g} . These coefficients express the relative significance of each g_α -function, and the prior PDF f_G is fully defined by solving Equation (2) with respect to μ_α , $\alpha = 1, 2, \dots, N_c$.

The next, specificatory, stage is an assessment of the observed data, χ_{data} . The χ_{data} values are recorded at a given set of m space-time points \mathbf{p}_i , $i = 1, \dots, m$, and they constitute the specificatory knowledge bases (S-KB). The S-KB might consist of hard data χ_{hard} , soft data χ_{soft} , or a combination of both as in this study.

In the final integration stage, the S-KB updates the G-KB. Blending the two knowledge bases yields the total given information $K = G \cup S$ about the stochastic process. The second fundamental BME equation illustrates the blending as

$$\int d\chi \xi_s e^{\boldsymbol{\mu}^T \mathbf{g}} - A f_K(\mathbf{p}) = 0, \quad (3)$$

where ξ_s is an operator that represents the S-KB, A is a normalization parameter, and f_K is the posterior PDF at each spatiotemporal point \mathbf{p} where prediction is sought. The subscript in f_K indicates that the posterior PDF is computed on the basis of the total information K . f_K is computed through Equation (3) and provides a complete stochastic description of the variable(s) of interest at a series of specified prediction locations \mathbf{p} . A variety of predicted attribute measures can be extracted from f_K to match the goals of the intended study, such as the distribution mean or mode. In our analysis, we predict the BME mean of transaction prices. To calibrate the BME results, we also map the transaction prices at the same space-time target locations using ordinary kriging. Rather than a PDF, kriging yields only predicted values and their associated prediction error.

Christakos (2000) shows that in the presence of only trend and covariance G-KB and the absence of soft data, the nonlinear BME predictor of Equation (3) reduces to the kriging predictor. Since this is the G-KB case in this article, we performed an experiment of hardening our soft data to use them with kriging by selecting the middle point of each soft interval as a single value. Naturally, this shortcut deprives the kriging analysis of the soft data uncertainty content that BME accounts for. Moreover, hardening might be conceptually entirely intractable when soft data have more elaborate distributional forms. As provisioned by theory, by applying the hardening shortcut we find that BME and kriging produce nearly identical predictions (results not provided). In the following, we illustrate the general scenario where soft data are not integrable by kriging to demonstrate the BME value for real estate mapping. In the next section, we describe how we compare BME to kriging and other test designs.

3. Experimental design

3.1. Data

We model house prices in Tarrant County, Texas, from January 2009 to December 2012. The larger study area covers a rectangular domain where Easting ranges between 715,150 and 719,750 m and Northing ranges between 2,127,400 and 2,136,400 m within the Texas North-Central State Plane Coordinate System. The area is northeast of the Fort Worth central business district and measures 4,600 by 9,000 m. There are a total of 1,901 homes that transact during the sample period. Due to multiple sales of the same property, the sample area yield is 2,420 transactions during 2009–2012. [Figure 1A](#) shows the geographical outline of Fort Worth and the study area.

We use these Texas data because the local market did not experience the unprecedented price volatility like other areas in beginning of the 21st century. Our choice mitigates the fact that dramatic price increases followed by significant decreases in local real estate markets may produce test findings that do not generalize to more typical markets. As example, the S&P/Case-Shiller index of US house prices increased at a continuously-compounding rate of 9.4% per year from January 2000 to the apex in July 2006. Florida, California, and Arizona markets experienced even higher appreciation rates. The national price index subsequently decreases by 5.3% per year from the 2006 high to the low in March 2012. In contrast, the Dallas/Fort Worth index from S&P/Case-Shiller exhibits an annual continuously-compounding increase of 3.5% from January 2000 to July 2006 and then an annual decrease of 1.6% from July 2006 to March 2012. These price changes are much more consistent with expectations of typical market conditions.

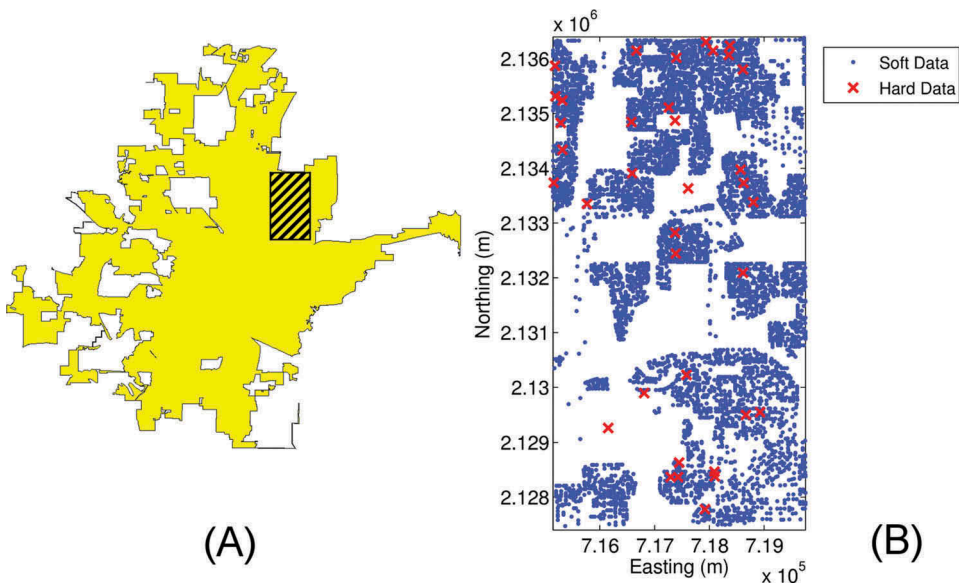


Figure 1. (A) The Fort Worth area in Tarrant County, Texas; the striped rectangle shows the study area. (B) Locations of tax assessed (soft data) values and transaction prices (hard data) in the study area in January 2010.

The observed transaction prices are the hard data in our analysis. We also use the assessed values from the local property tax office as soft data. Tax assessed values are generally publicly available for almost every property in the US. Our test method thus accounts for the fact that most market participants do not have ready access to numerous transaction prices, which are found in bulk in (generally inaccessible) proprietary databases of realtors or may be available as singular observations in public records. In contrast, tax offices provide the current property tax digest of all properties in the local market as a data panel, often online.

When compared to transaction prices and the underlying fair market value, the appraisal values should be considered as measured with uncertainty due to three reasons. The first is that property tax studies like Plummer (2015) find inequity and a lack of uniformity in assessments across properties. A second reason is that assessed values often lag transaction prices. For instance, when sales occur, Texas assessors mark the properties to the sale prices. If a property has not sold recently, assessors are expected to reassess values every 3 years. Some states have longer periods like Rhode Island, which is every 10 years, while others have no time provision (e.g., New York). Without a sale, assessed values will experience a lag. The third reason assessed values should be viewed as soft data is that tax assessors follow the formal appraisal process, which is not a negotiated arms-length transaction. While an appropriate process, appraisal-based prices are not believed to accurately reflect fair market values because information is not fully updated in the valuation process (Quan and Quigley 1991, Cho *et al.* 2014).

Since tax-assessed values are soft data, we need to establish the relation between them and transaction prices. Instead of a simple correlation, we regress transaction prices against the tax values and other property characteristics that are public information in the Tarrant county assessor's database. The additional independent variables are the size of the living area, the number of bedrooms and bathrooms, the garage capacity, and the home age along with binary variables for 5 realtor-defined geographical areas. Table 1 details the slope coefficients of the model parameters using heteroscedasticity-consistent standard errors. Because the assessed values should be close in magnitude to transaction prices, we note a strong model fit. The parameter estimate of 1.04 on the tax

Table 1. Transaction price model (\$).

Variable	Parameter estimate	<i>p</i> -Value
Tax assessed value (log price \$)	1.04	0.00
Living area (square feet)	−3.34	0.12
Number of bedrooms	−628.63	0.49
Number of bathrooms	858.65	0.48
Garage capacity (number of spaces)	6,088.86	0.00
Home age (years)	−112.07	0.02
Realtor-defined area 127	913.00	0.62
Realtor-defined area 128	−2,661.31	0.14
Realtor-defined area 129	−2,248.32	0.53
Realtor-defined area 130	−125.54	0.95
Intercept	−11,072	0.02
Number of observations	1,901	
<i>F</i> statistic	6,264.56	
Adjusted <i>R</i> ²	0.97	

Note: Realtor-defined area 126 is the control group.

assessed value indicates that transaction prices are approximately 4% higher on average than the property tax prices during the sample period.

After fitting the regression model, we compute the upper and lower 95% confidence intervals for an individual estimation using the standard error of the forecast, which accounts for the uncertainty in the regression line and the individual observation (as opposed to the standard error of the prediction, which accounts for uncertainty in the regression line only). We then compute the mean of both the lower and upper confidence intervals and use it to specify the price model uncertainty as a percentage of the model estimates values. For each model-estimated value, this percentage determines the lower and upper bound of the value. The bounds constitute an interval soft datum where the transaction price variable can take any value within this range. Our soft data base consists of interval values for 66,908 homes.⁵

Figure 1B shows the hard and soft data locations in January 2010. To better distinguish between soft data locations, we only show about 40% of those in Figure 1B. The figure shows how the soft data outline the housing subdivisions and neighborhoods and the dwarfing effect the soft data have on the hard data.

3.2. Experimental setup

We examine two test cases. In Case A, we use a sample with observations between the 25th and 90th percentile of transaction prices. This refinement reflects the fact that homes in similar price ranges usually represent complementary size, quality, and condition characteristics, which make them good comparable sales. They will thus be good predictors in building an index or understanding general price movements. This is similar to the requirement of appraisers to find transactions similar to the subject property being appraised. The refinement at the 25th and 90th percentile accomplishes this objective. The observations we consider in Case A still exhibit some price variability but are more homogeneous with 2–3 bathrooms, 3–4 bedrooms, 1–2 garage spaces, 1,600–2,600 square feet in size, and transaction prices ranging from \$100,000 to \$250,000. The price filtering in Case A produces a sample that is not significantly skewed (see Figure 2) such that we are able to model transaction prices using the observed levels.

In Case B, we use input from the same sample as in Case A to examine intra-neighborhood price variability. In contrast to the small scale, there exist price indices for large metropolitan areas. For instance, the Federal Housing Finance Administration provides an index for the top 100 metropolitan statistical areas (MSAs), which includes smaller cities with populations greater than 500,000. This still leaves over 750 smaller MSAs and micropolitan statistical areas.⁶ Furthermore, there are no price indices of smaller areas such as neighborhoods. Due to the ability to incorporate property tax values, BME is well suited to model a small spatial field.

First, we investigate the incidence of space–time surface trends in both the hard and soft data for the two test cases. In spatiotemporal mapping, the existence of surface trends can obscure underlying correlations in the scale of interest (Chilès and Delfiner 1999). The surface trend in our cases is a base price component at the local level as well as macroeconomic conditions such as US interest rates at the national level. We retain the trend values until the end of the prediction process and then restore them to obtain the actual transaction prices at all space–time locations.

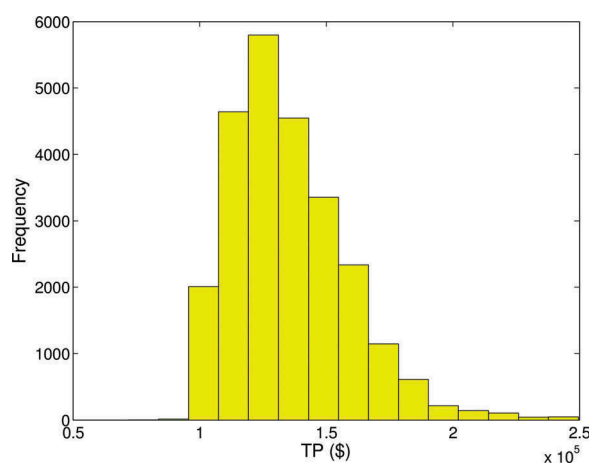


Figure 2. Histogram of sample used in Case A.

We obtain the surface trend through a moving-window exponential filter that leaves transaction price fluctuations around zero. The filter uses ranges that extend spatially to approximately a fourth of the size of the domain and temporally to approximately 12 months. When detailing the results in the next section, we include in the descriptive statistics the part of the total variability in the data which can be linked to the surface trend. The percentage variability is quantified as $V_{tr} = \left(1 - \frac{V_R}{V_T}\right)$, where V_T is the total variance prior to trend removal and V_R is the remaining variance. The magnitudes range from about 50% to 67%.

After saving off the trend components, the residual values are used to compute empirical estimates of the spatiotemporal covariance function on the S-TRF. Spatiotemporal covariances are mathematical constructs that must adhere to the criterion of positive definiteness (Christakos 1992). They can be modeled by functions relevant to the physical problem under study (see, e.g., Kolovos *et al.* 2013) or more commonly by simple functional forms such as the exponential or the Gaussian (e.g., Cressie and Wikle 2011). Spatiotemporal covariances are also commonly distinguished into having separable or non-separable spatial and temporal components (Kolovos *et al.* 2004). Our study establishes spatiotemporal correlation of the housing prices by using simple, non-separable covariance models, as shown in the following section. Upon determining the optimal structure, BME and kriging predict the transaction price residuals, and the surface trends are restored to create price maps. The outcome is a complete series of predicted housing values on predefined grid nodes for every month in the study period.

Our transaction price prediction is tested by means of a modified ‘leave-*n*-out’ cross-validation task for each month in 2012. Specifically, we conduct validation testing that is realistic in the context of the housing market: For each month we predict transaction prices at a select subset of data locations by excluding all data from the current and remaining future months, thus relying only on data from past instances. This is essentially an out-of-sample approach, where the predictive accuracy is measured by computing three validation statistics: the mean absolute error (MAE)

defined as $\frac{1}{N} \sum_{i=1}^N |x_i - \hat{x}_i|$, the mean relative error (MRE) defined as $\frac{1}{N} \sum_{i=1}^N \frac{x_i - \hat{x}_i}{x_i}$, and the absolute relative error (ARE) defined as $\left| \frac{x_i - \hat{x}_i}{x_i} \right|$. For each measure, N predicted values \hat{x}_i are compared to the corresponding observed values x_i to determine the error level.

4. Empirical results

4.1. Subsample of more homogeneous properties

For both BME and kriging, we predict transaction prices on a rectangular spatial grid of 47×91 nodes across 48 months, which is a spatiotemporal grid of 205,296 nodes. The spatial nodes are equidistant in the horizontal and vertical directions at 100 m, and the temporal interval is 1 month.

The Case A refinement of the entire transaction set produces a sample of homes with more similar properties that comprises of 718 hard data observations and 24,294 soft observations. By using a subset of the entire sample, this refinement leads to reduced data variability and a more accurate regression fit in the construction of soft data. Specifically, the uncertainty interval in soft data is $\pm 15\%$. Table 2 provides the descriptive statistics.

Table 3 details the Case A space–time covariance models. Note that the models for BME feature much longer temporal correlation ranges, and hence offer temporal prediction ability that goes farther in time than the hard data-based model used by kriging. This is attributed to the abundance of information in the soft and hard data that determine correlation for BME. The kriging covariance model is a relatively simple single nesting in space and in time.

Table 2. Case A descriptive statistics.

	BME	Kriging
Sample size	25,012	718
Minimum (\$)	79,140	100,000
Maximum (\$)	249,623	245,000
Mean (\$)	135,278	141,424
Standard deviation (\$)	23,000	27,604
Skewness	1.02	1.14
Kurtosis	4.56	4.69
Median (\$)	131,200	136,950
V_{tr} (%)	60.65	52.74

Table 3. Case A covariance models.

Analysis technique	Nested model	Spatial structure	Temporal structure	Sill c (\$^2\$)	Spatial range ρ (m)	Temporal range τ (months)
BME	1	Nugget	Spherical	1.0e8		99.30
	2	Exponential	Spherical	1.0e8	78.32	155.00
Kriging		$C(r, \tau) = c_1 \left[1 - \frac{3 t }{2\tau_1} + \frac{ t ^3}{2\tau_1^3} \right] + c_2 \exp\left(-\frac{r}{\rho_2}\right) \left[1 - \frac{3 t }{2\tau_2} + \frac{ t ^3}{2\tau_2^3} \right]$				
	1	Exponential	Spherical	3.6e8	180.02	15.17
			$C(r, \tau) = c_1 \exp\left(-\frac{r}{\rho}\right) \left[1 - \frac{3 t }{2\tau} + \frac{ t ^3}{2\tau^3} \right]$			

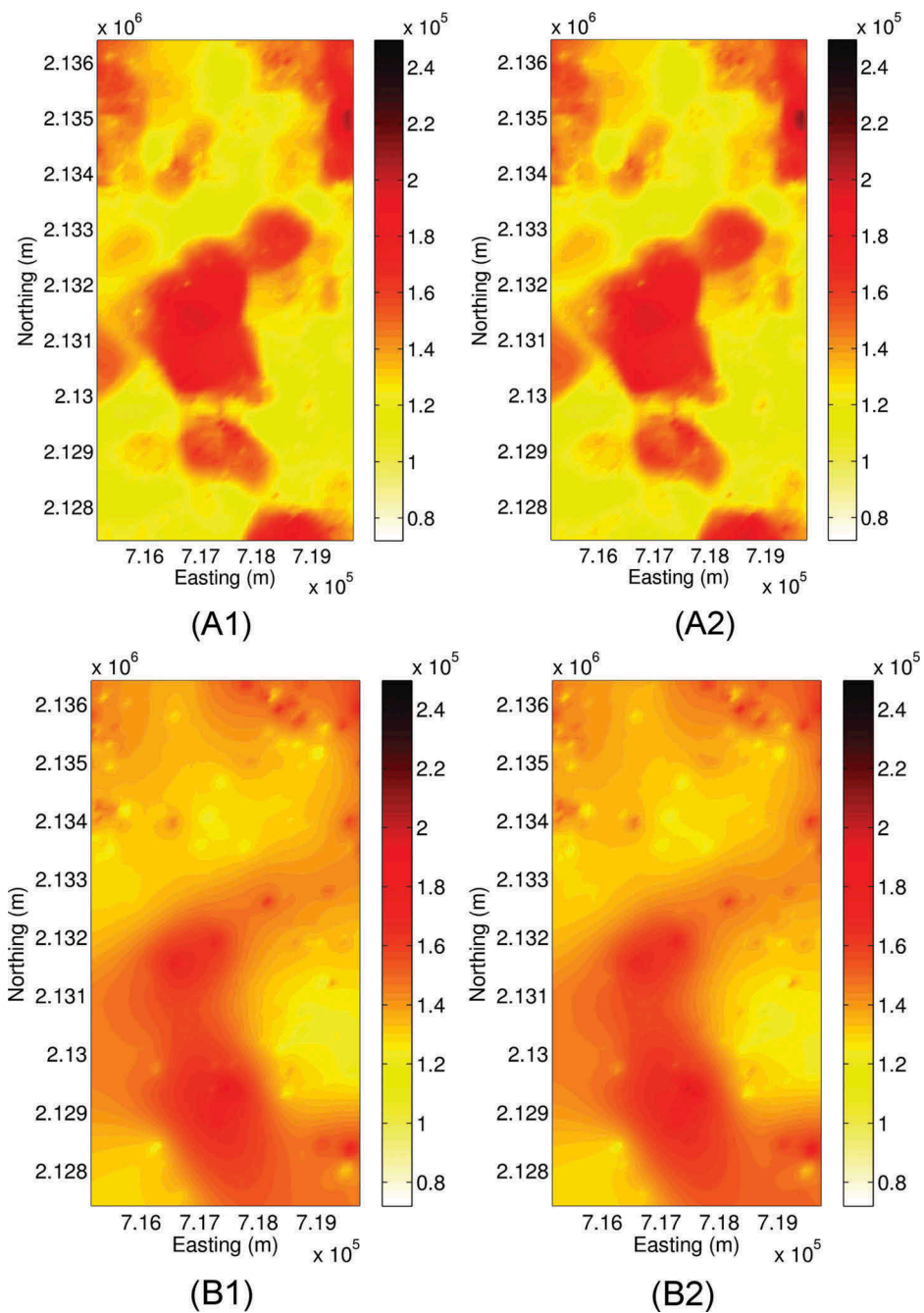


Figure 3. Predicted transaction prices for Case A: (3A) shows BME prediction for (A1) April 2009 and (A2) May 2009. (3B) shows kriging prediction for (B1) April 2009 and (B2) May 2009.

The plots in [Figure 3](#) map the BME and kriging predicted prices for the months of April and May 2009. We note the multiple levels of color and greater detail in the BME maps of [Figure 3A](#) compared to the kriging maps in [Figure 3B](#). In contrast, the kriging results are coarser and feature a smoother prediction surface where the data locations

are rather more distinguishable throughout the domain than in the BME maps. The point is that hard data alone produce lower quality inference compared to using secondary information, even if the latter is uncertain.⁷

Another set of prediction results support this finding. Given that G-KB input is means and covariances, the BME analysis produces a Gaussian prediction PDF at every output location. The standard deviation of the BME PDFs has a maximum value of \$14,427. The corresponding kriging prediction error is \$18,963. One might reasonably expect the soft data uncertainty to contribute to higher BME prediction error. However, the errors demonstrate that the relatively low soft data uncertainty level of 15% in Case A works synergistically with the abundance of soft data to result in lower prediction error levels for BME.

Table 4 and Figure 4 detail further performance information and error metrics using year 2012 results. In Panel A of Table 4, the MAEs and MREs are generally balanced, if slightly overall lower for BME. However, the validation analysis in Panel B indicates clearly stronger performance for BME. In particular, BME achieves AREs that are equal to or less than 10% error for 83.72% of the total validation points. The corresponding kriging score is 66.69%, or about at 4/5 of the BME performance. Figure 4 illustrates the ARE distributions. Thinner and taller curves centered at zero designate better performers, because they indicate that more validation relative errors are around zero. The plot shows clearly BME's increased accuracy compared to the kriging results. Additionally, the plot suggests that kriging exhibits a slight negative bias as its prediction tends to exceed the observed value.

In a realistic scenario where market participants will want to focus their understanding of prices on particular properties and attributes that fit within their budget and preferences, the Case A results demonstrate that available public data enhance our understanding of price variability at an inter-neighborhood level. We next investigate a finer scale.

Table 4. Case A error metrics.

Month	Mean absolute errors and mean relative errors			
	MAE (\$)		MRE (%)	
	BME	Kriging	BME	Kriging
January	17,108.86	19,113.75	-1.65	-7.43
February	8,844.30	7,205.73	1.61	-1.56
March	16,194.10	15,802.41	-0.44	-1.72
April	14,835.48	11,890.95	2.28	1.99
May	13,915.95	13,190.73	2.78	-0.39
June	9,040.79	14,586.61	-1.26	-4.87
July	11,924.45	15,621.73	3.72	-0.35
August	13,344.60	14,246.72	0.76	-0.85
September	17,224.21	14,824.04	2.69	-1.38
October	15,360.89	16,312.42	-0.77	-3.32
November	12,388.27	12,476.14	0.73	0.51
December	13,823.62	13,251.16	-0.59	-5.60
Percentage of validation points				
ARE categories	BME		Kriging	
Less than 5%	29.43		22.78	
Between 5% and 10%	54.29		44.31	
Greater than 100%	0.07		0	

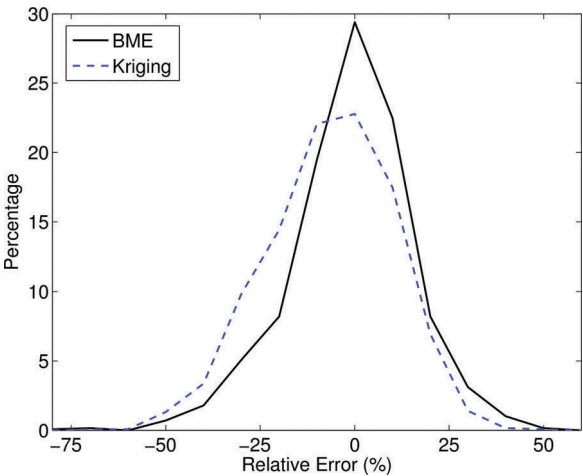


Figure 4. Count of validation points in relative error bins using Case A approaches.

4.2. Neighborhood scale

In Case B, we investigate a smaller spatial domain using a grid consisting of 51×51 nodes and spanning across 48 months, a total of 124,848 nodes. The spatial grid is twice as dense as the previous case with separation distances of 50 m in both of the Easting and Northing directions. The sample area is square with sides equal to 2,500 m (approximately 1.5 miles).

We find that only 111 properties transact within the smaller area over the 4-year period. These hard data are insufficient to conduct a kriging analysis per the practical empirical rules for geostatistical prediction; e.g., see Chilès and Delfiner (1999). In contrast, tax data exist for 4,193 homes, which is abundant information for BME prediction. Table 5 provides the descriptive statistics of the hard and soft data. Since the dataset in Case B is a local subset of the data used in Case A, the BME analysis uses the same space–time covariance model.

Table 6 details the year 2012 error metrics. In the absence of hard data to use kriging, we contrast Case B with the Case A results. Compared to Case A, the high density of input data enables us to downscale prediction in Case B by using a denser grid and gain more detail at the neighborhood-level prediction. We observe a reduction in MAEs for 4 months and a comparatively larger increase in the February, June and July MAEs. There are no statistics for the months April and November when data are not observed.

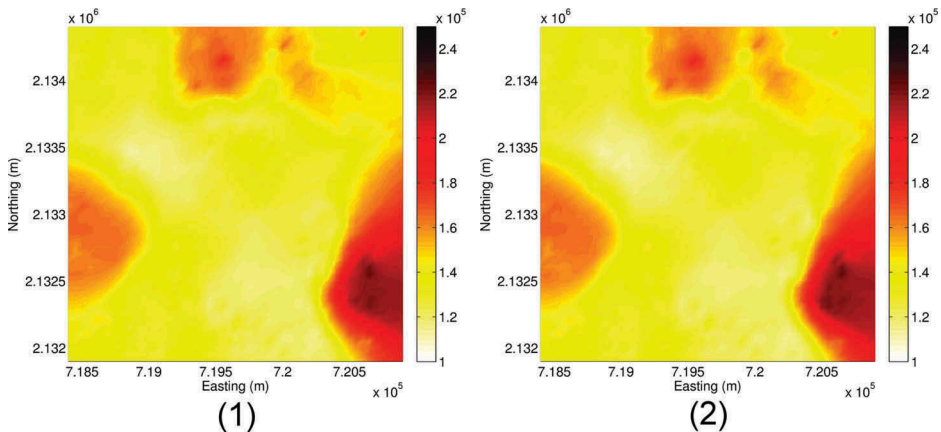
Table 5. Case B descriptive statistics using BME.

Sample size	4,304
Minimum (\$)	100,000
Maximum (\$)	249,800
Mean (\$)	137,809
Standard deviation (\$)	26,676
Skewness	1.58
Kurtosis	5.85
Median (\$)	130,350
V_{tr} (%)	66.20

Table 6. Case B error metrics.

Month	Mean absolute errors and mean relative errors	
	MAE (\$)	MRE (%)
January	15,594.78	-13.92
February	31,215.24	-28.38
March	13,377.30	-10.65
April	N/A	N/A
May	15,769.40	4.00
June	13,808.65	-1.09
July	23,940.64	9.35
August	14,262.87	-2.71
September	15,935.84	-14.49
October	15,277.72	4.63
November	N/A	N/A
December	14,083.59	4.95

Percentage of validation points	
ARE categories	Percentage of validation points
Less than 5%	27.27
Between 5% and 10%	57.58
Greater than 100%	0

**Figure 5.** Predicted transaction prices for Case B. Plots show BME prediction for (1) April 2009 and (2) May 2009.

The percentage of validation points at or below 10% error in Panel B of Table 6 is 84.85%, which is basically equivalent to the corresponding percentage 83.72% of Case A. Figure 5 portrays maps of BME mean predicted transaction values for Case B, again using April and May 2009.⁸

Overall, the map and statistics being similar to Case A are encouraging results because the Case B resolution is satisfactorily high for the real estate context. In contrast to kriging, which experiences insufficient input at this scale, BME proves most capable of conducting a space–time analysis at the intra-neighborhood level by using soft data.

5. Conclusion

Space and time form a continuum rather than existing as separate dimensions. In the scientific mapping of attributes like real estate prices that exist in both vectors, it is

imperative to correctly account for the spatiotemporal geometry. Otherwise, separate consideration of the spatial and temporal components can lead to insufficient representation and specious interpretation of space–time phenomena. To this end, we introduce pure spatiotemporal analysis in geostatistics-based real estate mapping. Our work illustrates for the first time how to characterize a real estate attribute from a spatiotemporal continuum perspective, investigate its correlation structure, and predict the attribute at unobserved locations.

Our analysis examines two cases of high practical interest in real estate mapping. Namely, one case centers on a focused large market category, and a second case analyzes prices at a more detailed neighborhood level. Our results highlight BME as a valuable tool for determining housing price indices on the basis of its capability to integrate soft data that contain nontrivial levels of uncertainty. In the first case, BME offered increased map detail and about 25% improvement in result accuracy compared to classical geostatistical prediction with kriging. Although computational burden scales with the number of data, the BME strong results mitigate the additional resources it consumes for the processing of soft data. However, improvement might be minimal in environments with numerous hard data. In this case, kriging improves its relative performance and can therefore make a preferable alternative to BME, as shown in a third case examined in the Supporting Information. Finally, in the case of neighborhood-level analysis BME demonstrated accurate predictive behavior using almost entirely soft information.

Our study exhibits a scientific pathway to describe the internal structure of real estate attributes in space–time. This pathway enables researchers to gain deeper understanding of market behavior by synthesizing knowledge from multiple relevant sources in a more rigorous fashion than previously available in real estate research. The mapping results demonstrate the local market behavior as it evolves across space and time, and can be valuable tools for assessment, analysis, planning, and management for both real estate researchers and practitioners in housing markets.

Notes

1. Journel (1989), Goovaerts (1997), and Chilès and Delfiner (1999) provide good starting points to understand geostatistics and the kriging family of techniques.
2. See Christakos (2000) for an extensive review of BME, and also in Christakos (2010, 2014) for conceptual perspectives of BME mapping in the context of critical reasoning and logic. Spatiotemporal BME has been applied in numerous studies and disciplines that illustrate its advantages and improvements (Yu *et al.* 2015). See examples in the fields of environmental and air pollution in Kolovos *et al.* (2002, 2010), disease modeling in Angulo *et al.* (2013), and renewable resources in Zagouras *et al.* (2015).
3. BME addresses other issues mentioned in the real estate literature. For instance, Pinkse and Slade (2010) noted that the normality assumption, endogeneity, and nonlinearity in the variable behavior cause significant challenges for the hedonic methods. BME makes no assumptions regarding the underlying data distribution and the predictor. Helbich (2015) is another example of spatial modeling that mitigates some of the issues of the spatial weight matrix. He uses fuzzy clustering and generalized additive hedonic model, the latter of which allows for nonlinear effects between the regressand and independent variables.
4. For our analysis, we use the BMElib library (Christakos *et al.* 2002) on Mathworks® Matlab. We performed the numerical tasks on an Intel® 6-core i7 desktop running Linux operating

system at 4.2 GHz. BMELib is available in BME/kriging software (Yu *et al.* 2007) free of charge at <http://seksgui.org>.

5. Tarrant County makes new assessments values publicly available at the end of each calendar year. Our method thus considers the tax assessed values as available to BME in the January of the following year. This is a sensible modeling perspective because it reflects the realistic situation that the assessment data are available to the entire market at the same time.
6. The Federal Housing Finance Administration produces price values for smaller cities down to populations of 10,000; however, to build these values, they use appraisal data. The appraisal data suffer from the same uncertainty and issues as the soft data we described in the preceding subsection.
7. Animations of the entire 48-month period (January 2009–December 2012) of predicted transaction prices are available as supplementary files on the journal website. See ‘mov1a-AbmePred.gif’ for BME and ‘mov1b-AkrigPred.gif’ for kriging.
8. Animation of the entire 48-month period (January 2009–December 2012) of predicted transaction prices is available as the supplementary file ‘mov2-BbmeSmallPred.gif’ on the journal website.

Disclosure statement

No potential conflict of interest was reported by the authors.

References

- Angulo, J., *et al.*, 2013. Spatiotemporal infectious disease modeling: a BME-SIR approach. *PLoS ONE*, 8 (9), e72168. doi:[10.1371/journal.pone.0072168](https://doi.org/10.1371/journal.pone.0072168)
- Banerjee, S., Carlin, B.P., and Gelfand, A.E., 2004. *Hierarchical modeling and analysis for spatial data*. Boca Raton, FL: Chapman & Hall/CRC.
- Chica-Olmo, J., 2007. Prediction of housing location price by a multivariate spatial method: Cokriging. *Journal of Real Estate Research*, 29 (1), 91–114.
- Chilès, J.P. and Delfiner, P., 1999. *Geostatistics-modeling spatial uncertainty*. New York, NY: John Wiley & Sons.
- Cho, Y., Hwang, S., and Lee, Y., 2014. The dynamics of appraisal smoothing. *Real Estate Economics*, 42 (2), 497–529. doi:[10.1111/reec.2014.42.issue-2](https://doi.org/10.1111/reec.2014.42.issue-2)
- Christakos, G., 1991. On certain classes of spatiotemporal random fields with application to space-time data processing. *IEEE-Trans on Systems, Man, and Cybernetics*, 21 (4), 861–875. doi:[10.1109/21.108303](https://doi.org/10.1109/21.108303)
- Christakos, G., 1992. *Random field models in earth sciences*. San Diego, CA: Academic Press.
- Christakos, G., 2000. *Modern spatiotemporal geostatistics*. New York, NY: Oxford University Press.
- Christakos, G., 2010. *Integrative problem-solving in a time of decadence*. New York, NY: Springer-Verlag.
- Christakos, G., 2014. *Stochastic medical reasoning and environmental health exposure*. London: Imperial College Press.
- Christakos, G., Bogaert, M.P., and Serre, M.L., 2002. *Temporal GIS. With CD-ROM*. New York, NY: Springer-Verlag.
- Christakos, G., Hristopulos, D.T., and Bogaert, P., 2000. On the physical geometry concept at the basis of space/time geostatistical hydrology. *Advances in Water Resources*, 23 (8), 799–810. doi:[10.1016/S0309-1708\(00\)00020-8](https://doi.org/10.1016/S0309-1708(00)00020-8)
- Cressie, N. and Wickle, C.K., 2011. *Statistics for spatio-temporal data*. Hoboken, NJ: John Wiley & Sons.
- Dubin, R.A., 1998. Predicting house prices using multiple listing data. *The Journal of Real Estate Finance and Economics*, 17 (1), 35–59. doi:[10.1023/A:1007751112669](https://doi.org/10.1023/A:1007751112669)
- Gelfand, A.E., *et al.*, 2004. The dynamics of location in home price. *Journal of Real Estate Finance and Economics*, 29 (2), 149–166. doi:[10.1023/B:REAL.0000035308.15346.0a](https://doi.org/10.1023/B:REAL.0000035308.15346.0a)

- Goodman, A., 1977. A comparison of block group and census tract data in a hedonic housing price model. *Land Economics*, 53, 483–487. doi:[10.2307/3145991](https://doi.org/10.2307/3145991)
- Goovaerts, P., 1997. *Geostatistics for natural resources evaluation*. New York, NY: Oxford University Press.
- Helbich, M., 2015. Do suburban areas impact house prices? *Environment and Planning B: Planning and Design*, 42, 431–449. doi:[10.1068/b120023p](https://doi.org/10.1068/b120023p)
- Journel, A.G., 1989. *Fundamentals of geostatistics in five lessons*. Washington, DC: American Geophysical Union.
- Kolovos, A., et al., 2002. Computational Bayesian maximum entropy solution of a stochastic advection-reaction equation in the light of site-specific information. *Water Resource Research*, 38 (12), 1318–1334. doi:[10.1029/2001WR000743](https://doi.org/10.1029/2001WR000743)
- Kolovos, A., et al., 2004. On certain classes of non-separable spatiotemporal covariance models. *Advances in Water Resources*, 27, 815–830. doi:[10.1016/j.advwatres.2004.04.002](https://doi.org/10.1016/j.advwatres.2004.04.002)
- Kolovos, A., et al., 2010. Multi-perspective analysis and spatiotemporal mapping of air pollution monitoring data. *Environmental Science and Technology*, 44 (17), 6738–6744. doi:[10.1021/es1013328](https://doi.org/10.1021/es1013328)
- Kolovos, A., et al., 2013. Model-driven development of covariances for spatiotemporal environmental health assessment. *Environmental Monitoring and Assessment*, 185 (1), 815–831. doi:[10.1007/s10661-012-2593-1](https://doi.org/10.1007/s10661-012-2593-1)
- Kuntz, M. and Helbich, M., 2014. Geostatistical mapping of real estate prices: an empirical comparison of kriging and cokriging. *International Journal of Geographical Information Science*, 28 (9), 1904–1921. doi:[10.1080/13658816.2014.906041](https://doi.org/10.1080/13658816.2014.906041)
- LeSage, J.P. and Pace, R.K., 2009. *Introduction to spatial econometrics*. Boca Raton, FL: Chapman and Hall/CRC.
- Montero, J.M. and Larraz, B., 2011. Interpolation methods for geographical data: housing and commercial establishment markets. *Journal of Real Estate Research*, 33 (2), 233–244.
- Nappi-Choulet, I. and Maury, T.-P., 2011. A spatial and temporal autoregressive local estimation for the Paris housing market. *Journal of Regional Science*, 51 (4), 732–750. doi:[10.1111/jors.2011.51.issue-4](https://doi.org/10.1111/jors.2011.51.issue-4)
- Páez, A., Long, F., and Farber, S., 2008. Moving window approaches for hedonic price estimation: an empirical comparison of modelling techniques. *Urban Studies*, 45 (8), 1565–1581. doi:[10.1177/0042098008091491](https://doi.org/10.1177/0042098008091491)
- Pinkse, J. and Slade, M.E., 2010. The future of spatial econometrics. *Journal of Regional Science*, 50 (1), 103–117. doi:[10.1111/jors.2010.50.issue-1](https://doi.org/10.1111/jors.2010.50.issue-1)
- Plummer, E., 2015. The effects of property tax protests on the assessment uniformity of residential properties. *Real Estate Economics*, 42 (4), 900–937. doi:[10.1111/1540-6229.12080](https://doi.org/10.1111/1540-6229.12080)
- Quan, D.C. and Quigley, J., 1991. Price formation and the appraisal function in real estate markets. *The Journal of Real Estate Finance and Economics*, 4, 127–146. doi:[10.1007/BF00173120](https://doi.org/10.1007/BF00173120)
- Savelyeva, E., et al., 2010. Modeling spatial uncertainty for locally uncertain data. In: P.M. Atkinson and C.D. Lloyd, et al., eds. *geoENV VII—geostatistics for environmental applications: quantitative geology and geostatistics*. Springer: The Netherlands, 295–306.
- Yoo, E.-H. and Kyriakidis, P.C., 2009. Area-to point kriging in spatial hedonic pricing models. *Journal of Geographical Systems*, 11, 381–406. doi:[10.1007/s10109-009-0090-z](https://doi.org/10.1007/s10109-009-0090-z)
- Yu, H.-L., et al., 2007. Interactive spatiotemporal modelling of health systems: the SEKS-GUI framework. *Stochastic Environmental Research and Risk Assessment*, 21 (5), 555–572. doi:[10.1007/s00477-007-0135-0](https://doi.org/10.1007/s00477-007-0135-0)
- Yu, H.-L., Ku, S.-J., and Kolovos, A., 2015. A GIS-based tool for spatiotemporal modeling under a knowledge synthesis framework. *Stoch Environ Res Risk Assess*. doi:[10.1007/s00477-015-1078-5](https://doi.org/10.1007/s00477-015-1078-5).
- Zagouras, A., Kolovos, A., and Coimbra, C.F.M., 2015. Objective framework for optimal distribution of solar irradiance monitoring networks. *Renewable Energy*, 80, 153–165. doi:[10.1016/j.renene.2015.01.046](https://doi.org/10.1016/j.renene.2015.01.046)